

Vorhabensbezeichnung	Förderkennzeichen:
Deliverable 1.3.1 Charakterisierungsbericht zu allen Materialien / Characterization report for all nanoGEM materials.	Fällig am: M24 – Sept. 2012
Verantwortlich: Bryan Hellack, Tim Hülser, Emilia Izak, Thomas Kuhlbusch, Frank Meyer, Mathias Spree, Matthias Voetz, Hartmut Wiggers, Wendel Wohlleben (BASF, Bayer Technology Services, ItN Nanovation, IUTA)	

This pdf is the public version of an internal deliverable. We document here the methods used for physical-chemical characterization of the nanoGEM materials, and we present key results by comparing materials.

However, this document does not contain complete characterization results for all nanoGEM materials. These are contained in the datasheets accessible on the nanoGEM intranet.

## 1. Rationale: systematic surface functionalization with reference materials

Nanomaterials with commercial relevance were selected for nanoGEM. These products are directly synthesized in suspension with polymer coatings that optimize the processability and performance for the final industrial application (AP1.1). In contrast to the agglomerated powder materials in NanoCare, the nanoGEM materials are near-perfectly individualized nanoparticles in their as-produced state, although changes of their colloidal properties will be induced by the testing media (as investigated by APQ).

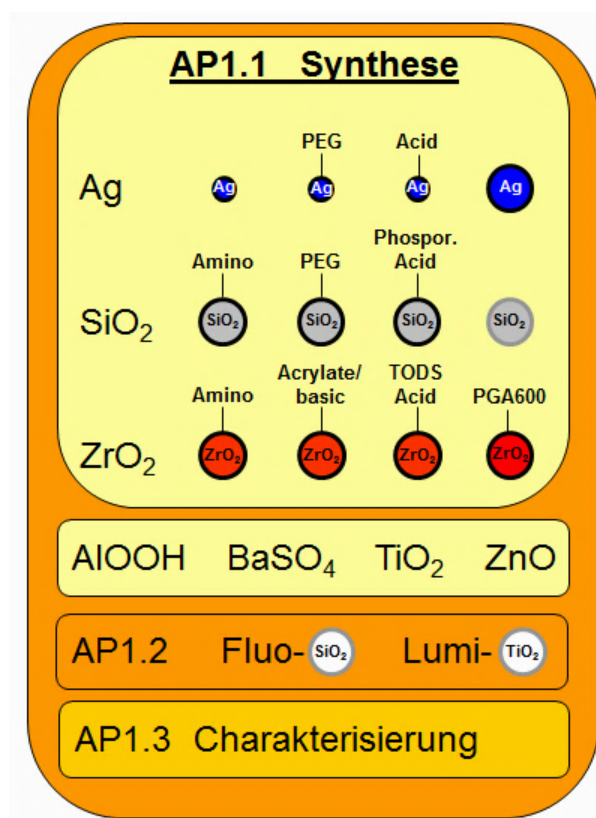
- $\text{ZrO}_2$  finds consumer-relevant applications in self-cleaning coatings in stoves. The nanoscale formulation is essential for this functionality.
- Ag is the dominant material for the conductive wires that collect the photovoltaic charge carrier on Si modules. The nanoscale formulation is advantageous for the formation of thinner wires with reduced shadowing and enhanced Si module efficiency.
- $\text{SiO}_2$  is the most widely used filler for coatings, and is introduced to plastics. The nanoscale formulation is essential to control the mechanical properties at retained high optical quality.

While also the commercially most relevant formulations were included in nanoGEM, additional materials with the identical nanoparticle core but systematically varied polymer surface modifications were synthesized and distributed. Some of these modifications were chosen to be closely matched with different cores, some are were selected to span the widest possible range of surface properties. For Ag nanoparticles, monodispersed samples of different sizes but identical surface add another axis to the systematic comparisons. During the course of the nanoGEM project, some of the originally planned surface modifications could not be realized in sufficient purity, and were replaced by analogous materials that retain the systematic variation.

Additionally, four reference materials were acquired from the OECD sponsorship program or contributed directly by industrial partners. These materials ( $\text{TiO}_2$ ,  $\text{AlOOH}$ ,  $\text{ZnO}$ ,  $\text{BaSO}_4$ ) were investigated in detail in the NanoCare project, and were re-characterized with the latest nanoGEM methods.

As another specialty, two routes to luminescent nanomaterials were explored (AP1.2). Both SiO<sub>2</sub> suspension (analogous to one of the AP1.1 materials) and TiO<sub>2</sub> powder (analogous to one of the reference materials) were evaluated and applied in AP3, and the powder form is presently scaled up for an inhalation-biokinetics study in AP3.

The resulting material's matrix is a unique asset of nanoGEM among any other European or national nanosafety project.



The characterization in AP1.3 was originally planned according to the OECD sponsorship program endpoints.(OECD 2009) In the meantime, ECHA has delivered the nano-specific Appendix R7.1 to the REACH guidance,(ECHA 2012) and the nanoGEM data sheets and characterization methods were checked to be compatible with the recommended protocols. All materials (surface-modified suspensions, reference powders, luminescent) were characterized according to standardized endpoints with documented methods.(Wohlleben et al. 2013)

The data sheets are available in the nanoGEM intranet.

The following Table summarizes the materials that were distributed to the nanoGEM partners, some in several reproductions after the initial delivery, since it is an intrinsic property of the suspensions to be more fragile than powders against year-long storage.

Nanomaterial	Form: Powder (P)/ Dispersion (D)	Supplier	Plan	Delivered	Data Sheets (online)
nanoGEM_Böhmit (AlOOH)	P	BTS	M1	03-2011	03-2011
nanoGEM_BaSO <sub>4</sub> (= NM220)	P	Solvay	M1	07-2011	06-2011
JRC_TiO <sub>2</sub> P25 (= NM105)	P	Mercator	M1	10-2011	02-2012
JRC_ZnO (= NM111)	P	Mercator	M1	10-2011	10-2011
nanoGEM_Eu@TiO <sub>2</sub>	P	IUTA	M6-9	03&06-2011	09-2011
nanoGEM_Si@SiO <sub>2</sub>	D	IUTA	M6-9	?	?
nanoGEM_SiO <sub>2</sub> .FITC	D	BTS	M6-9	03-2011	08-2012
nanoGEM_Ag_50	D	BTS	M1	12-2010	07-2011
nanoGEM_Ag_50.PEG*	D	BTS	M3	-	-
nanoGEM_Ag_50.mono	D	BTS	(M1)	02-2012	04-2012
nanoGEM_Ag_50.citrat	D	BTS	M6	09-2011	02-2012
nanoGEM_Ag_200	D	BTS	M6	02-2011	03-2012
nanoGEM_Ag_200.mono	D	BTS	(M6)	10-2011	11-2011
nanoGEM_SiO <sub>2</sub> .naked	D	BASF	M1	10-2010	10-2010
nanoGEM_SiO <sub>2</sub> .PEG	D	BASF	M3	12-2010	12-2010
nanoGEM_SiO <sub>2</sub> .amino	D	BASF	M6	05&08-2011	05-2011
nanoGEM_SiO <sub>2</sub> .phosphat	D	BASF	M6	05&08-2011	05-2011
nanoGEM_ZrO <sub>2</sub> .TODS	D	ItN	M1	11-2010	04-2011
nanoGEM_ZrO <sub>2</sub> .acrylbas	D	ItN	M1	02-2011	04-2011
nanoGEM_ZrO <sub>2</sub> .amino	D	ItN	M6	07-2011	07-2011
nanoGEM_ZrO <sub>2</sub> .PGA600	D	ItN	M6	10-2011	03-2012

\*aggregated, not delivered

## 2. Reference materials from the OECD sponsorship program and from NanoCare (BMBF)

Within the NanoGEM project, four different types of reference materials were used. While each material provided reference data to compare the various experiments in general, two of the materials also made it possible to directly compare to results achieved in NanoCare, and thus connect to studies of the former project. In addition to that, two other materials were chosen to be supplied from the OECD sponsorship program, and connect to international reference studies.

While boehmite (AlOOH) had already been obtained by BTS in two different particle sizes within the NanoCare project, it now could be supplied to the NanoGem partners. Similar to the former project, BaSO<sub>4</sub> was provided by its manufacturer Solvay and distributed among the partners. Both OECD reference materials, TiO<sub>2</sub>P25 as well as ZnO, were obtained from Fraunhofer IME / Mercator and shared within the project.

All reference materials were completely characterized by BASF and BTS, and data sheets were compiled to be made available to the partners via the NanoGEM website.

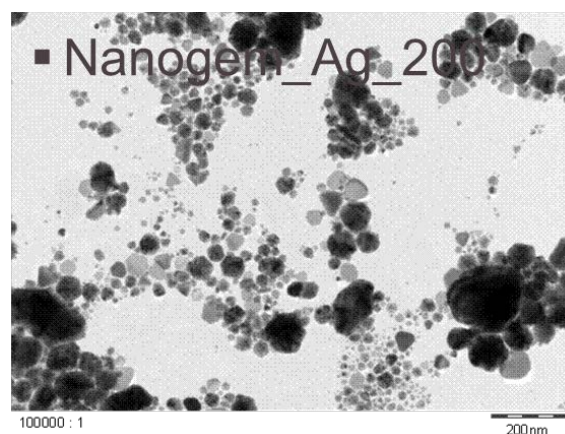
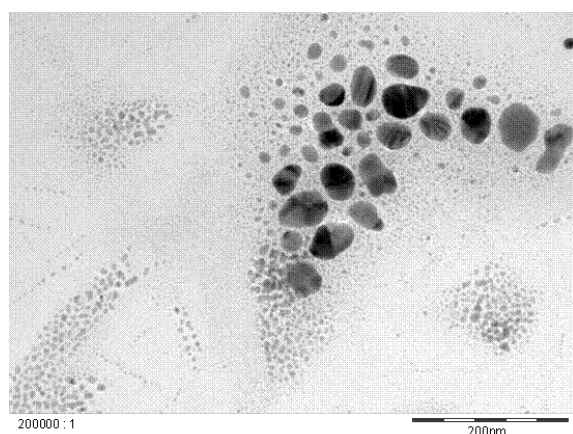
Nanomaterial	Form	Program	Supplier	Characterization
nanoGEM_Boehmite (AlOOH)	P	NanoCare	BTS	BTS
nanoGEM_BaSO <sub>4</sub> (= NM220)	P	NanoCare	Solvay	BASF, BTS
JRC_TiO <sub>2</sub> P25 (= NM105)	P	OECD	Mercator	BTS
JRC_ZnO (= NM111)	P	OECD	Mercator	BASF

## 1. Surface functionalized nano-Ag suspensions from Bayer TS

Probe	Surfactant	Name	Formula
Nanogem_Ag_50	Disperbyk 190	Blockcopolyether	
Nanogem_Ag_200	Disperbyk 190		
Nanogem_Ag_50_mono	Luvitec K90	Polyvinylpyrrolidone	
Nanogem_Ag_200_mono	Luvitec K90		
Nanogem_Ag_50_citrat	Citrate		
Nanogem_Ag_50_PEG	PEG 2000	Polyethylene glycol	

**3.1. Nanogem\_Ag\_50 and Ag\_200** are produced at Bayer as a semi-commercial Product. In the first approach, these silver particles were planned to be used within the Nanogem project.

Nevertheless, the dispersions showed very high polydispersity. To deliver monodispersed particles to the Nanogem partners, new ways of the synthesis were developed (Ag\_mono).

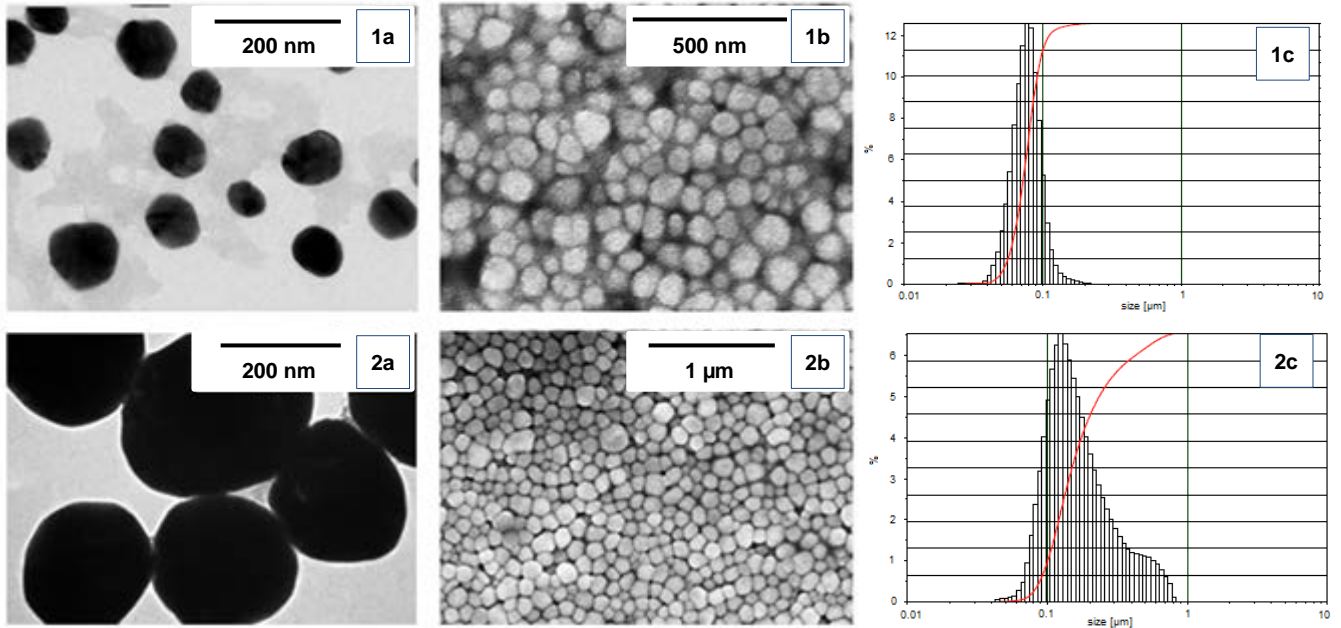


**3.2. Nanogem\_Ag\_50\_mono and Ag\_200\_mono** silver nanoparticles were synthesized using chemical reduction method. Silver nitrate ( $\text{AgNO}_3$ ) was used as the metal precursor. In the first step, silver oxide particles ( $\text{Ag}_2\text{O}$ ) were produced by reaction of  $\text{AgNO}_3$  with  $\text{NaOH}$ . Polyvinylpyrrolidone (Luvitec K90<sup>®</sup>) was used as a dispersive agent. In the next step,  $\text{Ag}_2\text{O}$  was reduced by FA to produce silver particles. To rid of an excess of the reagents, the NPs dispersions were centrifuged and washed 5 times with acetone, in 1:4 ratio, and 3 times with deionized water. The NPs were placed into an ultrasonic bath for 15 minutes and subsequently sonicated with 5 mm microtip for 5 minutes at 30 % amplitude.

The results of the NPs characterization are summarized in the table below.

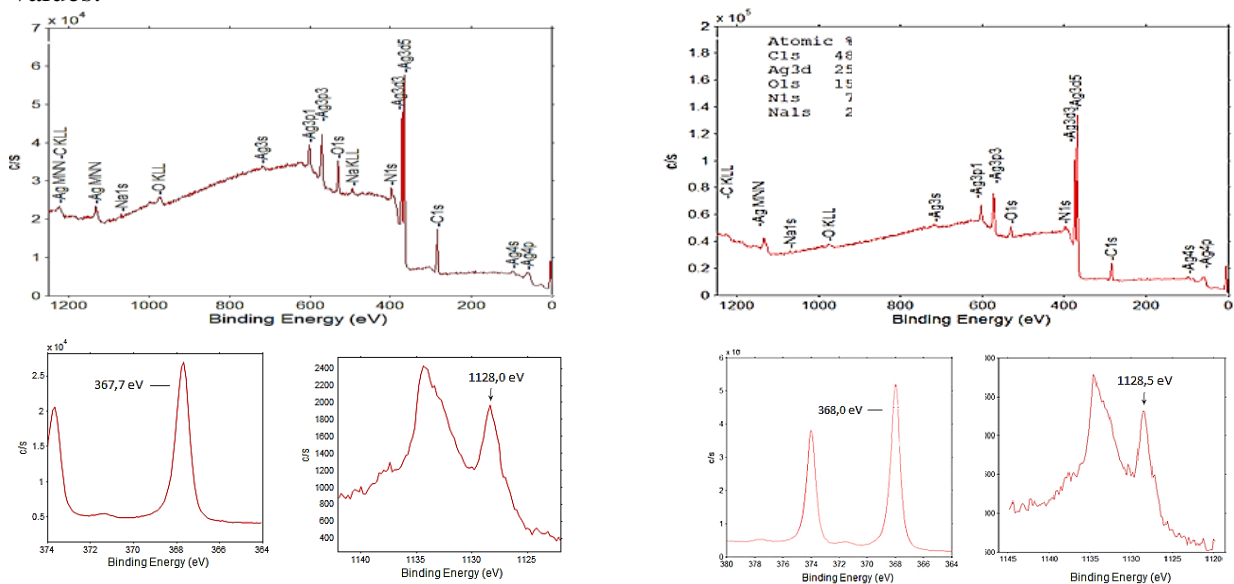
Name	Ag_50_mono (= Ag_PVP_80)	Ag_200_mono (= Ag_PVP_200)
Shape	Quasi spherical	Quasi spherical
Concentration	10 % (wt/wt)	10 % (wt/wt)
Size/size distribution & aggregation/agglomeration state	DLS-agglomerates size: 123 nm TEM: $d_{50}=79$ nm, $d_{90}=99$ nm AC: $d_{50}=77$ nm, $d_{90}=101$ nm	DLS-agglomerates size: 408 nm TEM: $d_{50}=134$ nm, $d_{90}=300$ nm AC: $d_{50}=95$ nm, $d_{90}=188$ nm
Crystal structure	Cubic	Cubic
Surface chemistry	XPS: Atom% C 59.1, O 17.5, Ag 15.9, Na 7.5 SIMS: Ag, Cl, $\text{C}_x\text{H}_y\text{O}_z$	XPS: Atom % C 77.2, O 10.7, Ag 0.4, N 11.7, Na 1.0 SIMS: $\text{C}_x\text{H}_y\text{O}_z$
Surface charge	Zeta potential: - 12.5 mV $\pm$ 0.5	Zeta potential: - 5.5 mV $\pm$ 0.5

SEM and TEM images showed a quasi-spherical shape and monodispersity of the NPs (figure below). The monodispersity was additionally proven by DLS and AUC measurements.



Silver nanoparticles characterization: (1) Ag<sub>50</sub>\_mono, (2) Ag<sub>200</sub>\_mono; (a) TEM, (b) SEM and (c) AC

The presence of PVP immobilized onto the NPs surface was indicated by XPS and SIMS analysis. XPS data additionally proved that all of the surface atoms were on Ag<sup>0</sup> state, confirming the absent of silver ions (Ag<sup>+</sup>). The negative charge observed with the zeta potential measurements was caused by PVP ionized form, which normally occurs at high pH values.<sup>1</sup>



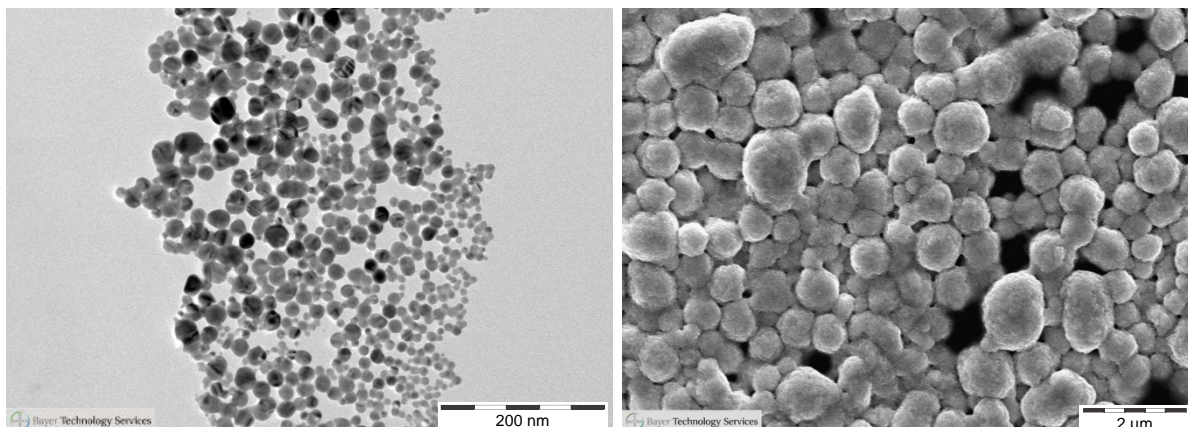
<sup>1</sup> Faibish R, Cohen Y: Fouling-resistant ceramic-supported polymer membranes for ultrafiltration of oil-in-water microemulsions. J Membr Sci, 2001,185: 129–143

**3.3. Nanogem\_Ag\_50\_citrat** was prepared in deionized water using  $\text{AgNO}_3$  as the metal precursor and sodium borohydride ( $\text{NaBH}_4$ ) as the reducing agent. Trisodium citrate ( $\text{C}_6\text{H}_5\text{O}_7\text{Na}_3$ ) was used as the stabilizer.

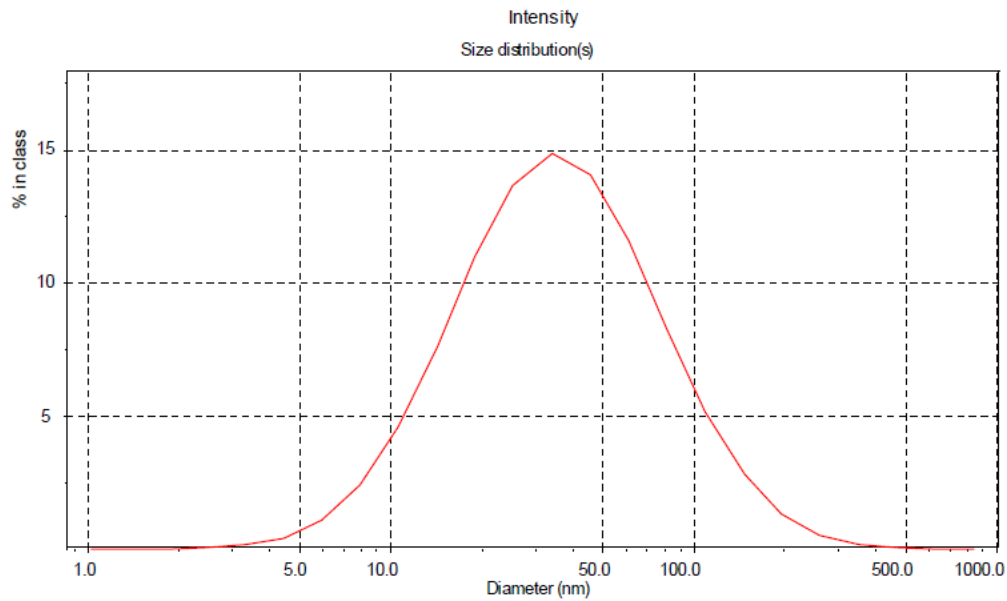
The results of the NPs characterization are summarized in the table below.

Name	Ag_50_citrat
Shape	Quasi spherical
Concentration	14.7 % (wt/wt)
Size/size distribution & aggregation/ agglomeration state	TEM: $d_{50}= 20 \text{ nm}$ , $d_{90}= 37 \text{ nm}$ AC: $d_{50}= 38 \text{ nm}$ , $d_{90}=56 \text{ nm}$
Crystal structure	cubic
Surface chemistry	XPS: Atom% C 21.2 O 14.8, Ag 62.1, Na 1.9 SIMS: Ag, Cl, Ca, F, Na, K $\text{C}_x\text{H}_y\text{O}_z$

TEM and SEM images of the silver NPs showed their quasi-spherical shape and smooth surface morphology. The NPs did not tend to agglomerate/aggregate.

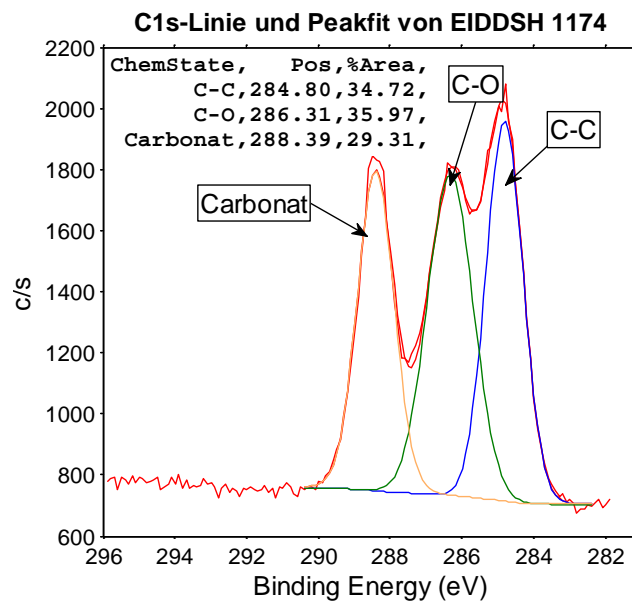


DLS measurements showed a broad NPs size distribution with maximum intensity of 35 nm.

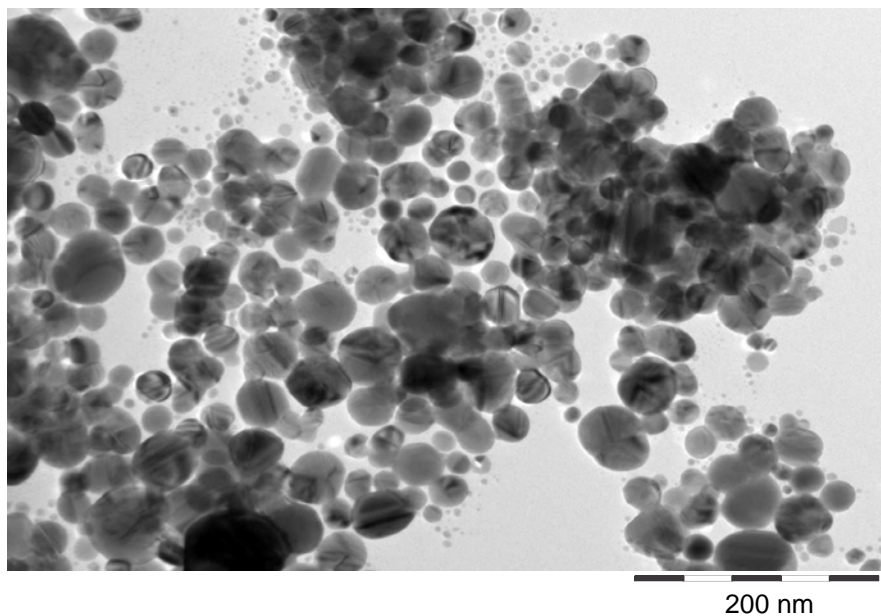


SIMS measurements indicated a presence of many impurities (Cl, Ca, F, Na, K  $C_xH_yO_z$ ), probably coming from the reagents itself or not properly clean reaction vessels.

**3.4. Nanogem\_Ag\_50-PEG** are modified silver particles with PEG on their surface. The particles were directly produced in PEG 200 solution acting as the solvent and as the surfactant. The  $AgNO_3$  was reduced by FA at  $60^\circ C$ . The XPS measurements (figure below) confirmed the presence of PEG molecules on the NPs surface.



Nevertheless, these particles were not stable. It was not possible to deliver them to the Nanogem partners because of the fast and strong aggregation.

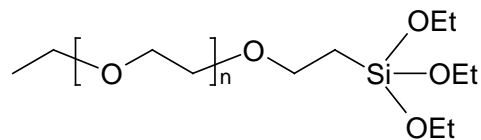


## 2. Surface functionalized nano-SiO<sub>2</sub> suspensions from BASF

Suspensions of amorphous SiO<sub>2</sub> are commercially available in large quantities and with very reproducible properties. Due to their synthesis they are intrinsically spherical and of rather narrow size distribution.

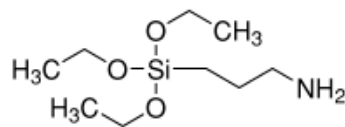
Since gelation can occur after months of storage, the nanoGEM project used multiple batches of non-functionalized SiO<sub>2</sub> (Levasil® 200, HC Starck), distributed as **nanoGEM.SiO<sub>2</sub>.naked**. The same material is the basis for a covalent functionalization at BASF with three different low-molar-mass silanes:

**nanoGEM.SiO<sub>2</sub>.PEG** has a Polyethylenglycol (PEG) of chain length M<sub>w</sub>=500g/mol

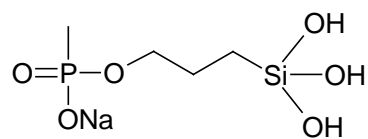


**nanoGEM.SiO<sub>2</sub>.amino** carries a positively charged NH<sub>2</sub> end group on a flexible, but short C3-linker:

The reagent used is aminopropyltrimethoxysilane (APTES)



**nanoGEM.SiO<sub>2</sub>.phosphat** carries a negatively charged PO<sub>3</sub> end group on the same C3-linker:

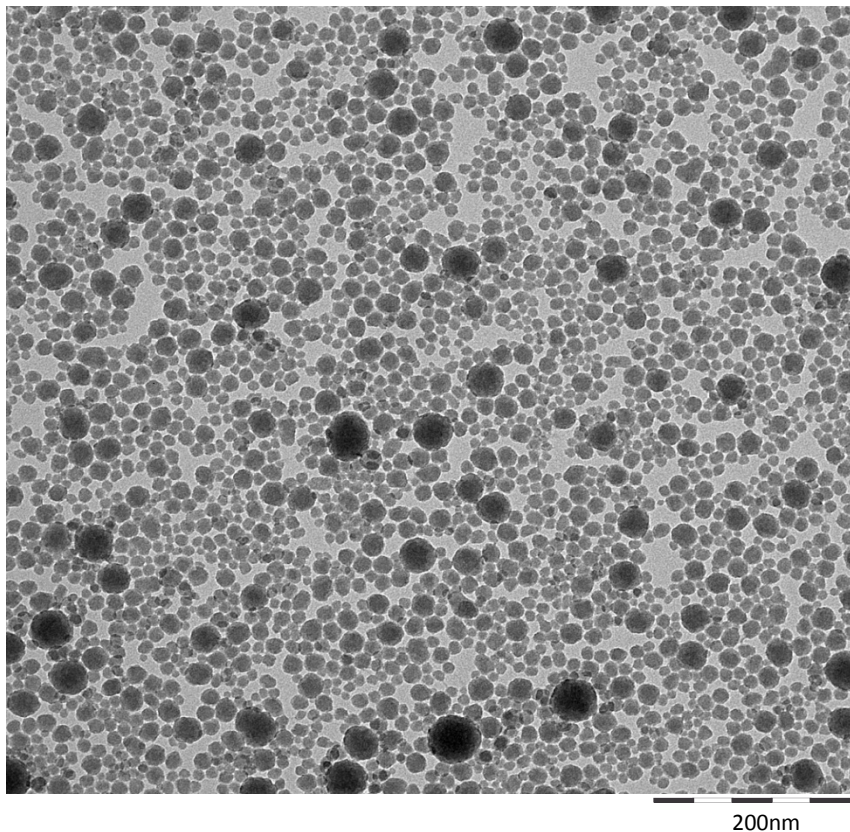


For every new batch, the size distribution in suspension (no agglomeration) and the electrophoretic mobility with pH titration (successful surface modification) were checked for reproducibility, with only 2 of 15 reproductions failing.

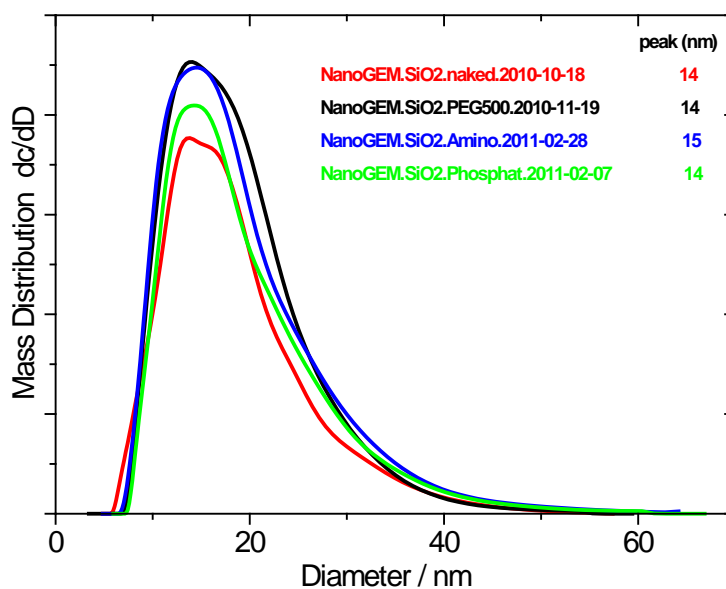
All samples were sterilized by gamma-irradiation (30 Gy) at WWU before distribution.

REACH-relevant *endpoints* are highlighted in the following.

The *representative TEM image* after functionalization (here on nanoGEM.SiO<sub>2</sub>.PEG) confirms the retained spherical structure, no aggregates, no agglomerates, and no secondary nucleation.



In a comparative plot, the *size distribution* is not significantly changed by the surface modification. The peak diameter at 14 nm is retained with at most 1 nm increase. This size reflects the primary particles, in excellent accord with the specified *BET surface* of 200 m<sup>2</sup>/g, which corresponds to a diameter of 15 nm. The *dispersability* in water is hence near-perfect.



In XRD, these particles have no diffraction peaks, confirming their amorphous structure, without indication of *crystallinity*

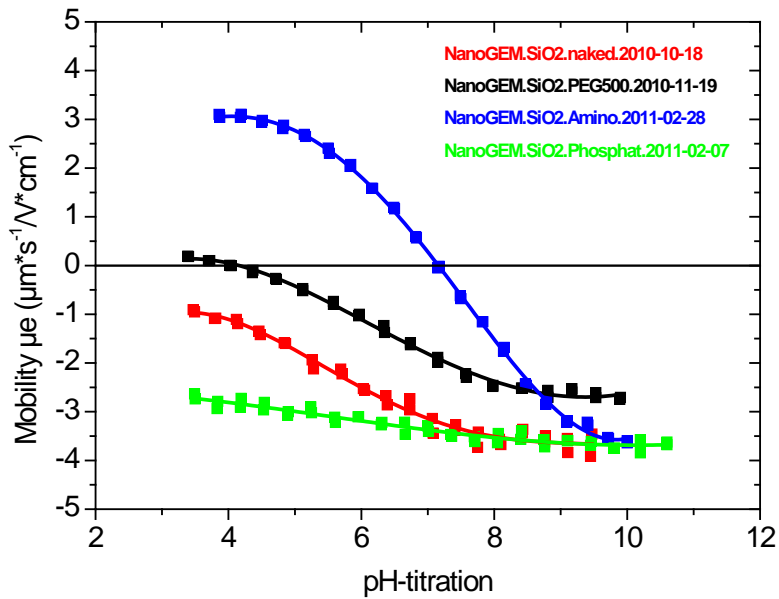
The as-tested (in situ) *degradation* of the nanoGEM.SiO2.naked and of the reference materials TiO<sub>2</sub> NM105 and BaSO<sub>4</sub> NM220 was investigated by incubation for 28d in phosphate-buffered saline (PBS, to simulate the surface of epithelium) or 28d in phagolysosomal simulant fluid (PSF, to simulate the lysosome of macrophages), or 1d in 0.1n HCl (to simulate oral uptake into the stomach) or 7d in a Simulated Intestinal Fluid (fasted state, FaSSIF). All incubation times were chosen at or above the maximum realistic residence time of nanomaterials in the specific body compartment, since we expected only weak dissolution effects. We found that the solubility of TiO<sub>2</sub> NM105 is below the detection limits in all media except PSF (simulating the lysosome of macrophages). However, the positive control nanoGEM.SiO<sub>2</sub> naked dissolves as expected, including the least aggressive medium of PBS (simulating lung deposition). The solubility of BaSO<sub>4</sub> NM212 in all media, including PSF, is vanishing against the positive control, and noticeable only in 0.1n HCl. All materials,

incl. TiO<sub>2</sub> NM105, undergo morphological changes by Ostwald ripening and recrystallization in PSF and HCl, but retain their crystallinity. In PSF, all tested material tend to gel, but especially nanoGEM.SiO<sub>2</sub>.naked loses its dispersed fraction while retaining its nanostructure. The lipids in FaSSIF tend to agglomerate the nanomaterials. The BaSO<sub>4</sub> NM220 is remarkable in its high dispersed fine fraction in all buffers.

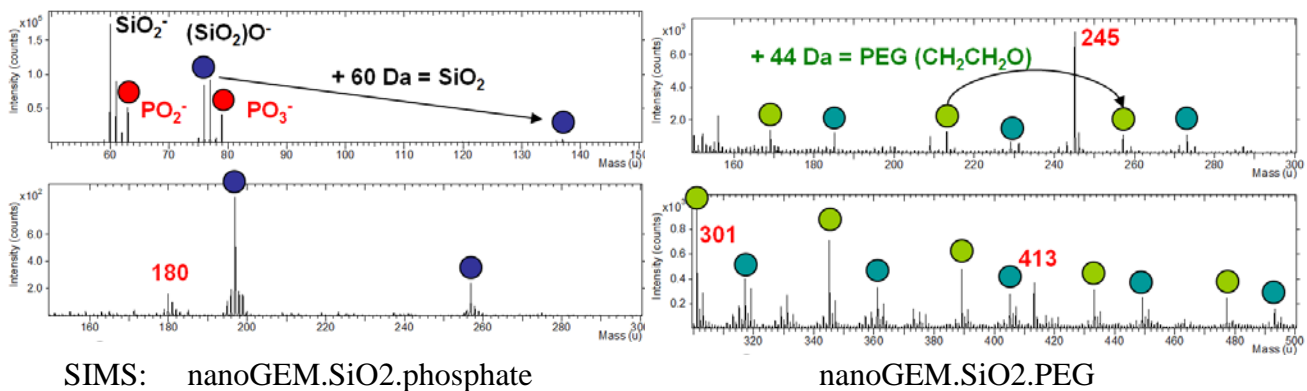
The full persistence / degradation results with colloidal and structural characterization have been reported independently.(Wohlleben et al. 2013)

	PBS_ 28d	PBS_ 28d	PBS_ 28d	PSF_ 28d	PSF_ 28d	PSF_ 28d	FaSSIF _7d	FaSSIF _7d	FaSSIF _7d	HCl_ 1d	HCl_ 1d	HCl_ 1d
	fine fraction / wt%	Dissolu- tion / wt%	charge zetapot / mV	fine fraction / wt%	Dissolu- tion / wt%	charge zetapot / mV	fine fraction / wt%	Dissolu- tion / wt%	charge zetapot / mV	fine fraction / wt%	Dissolu- tion / wt%	charge zetapot / mV
TiO <sub>2</sub> NM105	110	0	-23	6	0.15	-16	8	0	-32	33	0	38
BaSO <sub>4</sub> NM220	87	0.12	-33	37	0.07	-4	45	0.10	-42	0	1.02	17
SiO <sub>2</sub> . naked	82	1.18	-22	0	1.39	-1	36	0.55	-29	90	0.13	4

The successful functionalization is demonstrated by the *surface charge*, measured as electrophoretic mobility with pH titration. Clearly, the non-functionalized nanoGEM.SiO<sub>2</sub>.naked retains its negative charge from Si-OH groups across the relevant physiological pH range. At neutral pH, this mobility corresponds to a zeta potential of -49 mV. The nanoGEM.SiO<sub>2</sub>.phosphate is charged even stronger at acidic pH. In contrast, the charge is reduced for the nanoGEM.SiO<sub>2</sub>.PEG, with an isoelectric point at pH 4, and the charge is inverted to positive values for nanoGEM.SiO<sub>2</sub>.amino with an isoelectric point around pH 7.2 .



The *surface chemistry* molecular origin is highlighted by SIMS measurements of fragment ions from the top 1 to 3 nm of the nanomaterial's surface after washing with deionized water to remove any non-bound organic components, pelleting by hard sedimentation, drying (40,000 rpm for 2h, nanoGEM SOP SIMS).

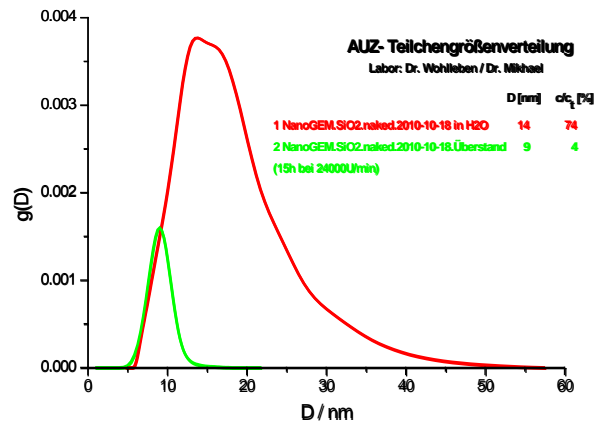


SIMS: nanoGEM.SiO2.phosphate

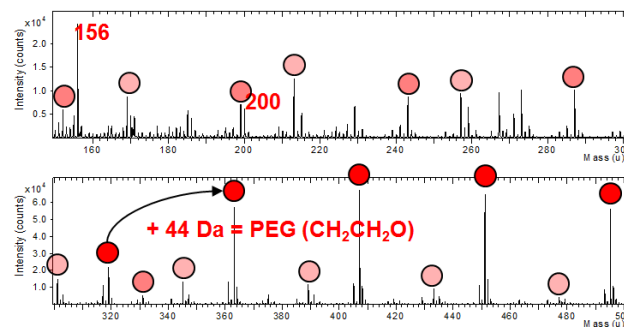
nanoGEM.SiO2.PEG

The characteristic SiOx fragments are still visible in the negative ions (left panel, on nanoGEM.SiO2.phosphate), indicating a partial coverage of the surface. But also the POx fragments are clearly detected, as expected. Positive ions (right panel, on nanoGEM.SiO2.PEG) clearly demonstrate the characteristic PEG fragments bound to the surface. On the selected example of nanoGEM.SiO2.naked, inverse gas chromatography reveals a highly polar surface.

In order to identify any *impurities* we characterized the supernatant (a.k.a. Überstand, Nullprobe) after a hard sedimentation (24,000 rpm, 15h). First, we verified that this procedure has indeed removed the particles. By Analytical Ultracentrifugation, the same method that was used for all data sheets, we can quantify both size range and absolute concentration of the remaining particles. The results demonstrate that as expected the larger particles are removed preferentially, with between 95% and 98% of the particles removed.



The chemical identification of the supernatant by SIMS shows the some fraction of the functionalization agent has indeed not grafted onto the particle surface, but is present as freely dissolved organics, especially for the PEG agent, less for the other agents.



Note that SIMS is not a quantitative technique. The absolute concentration of free functionalization agent is estimated from Interference-AUC to be 0.4% in the original sample with 20% particle content, i.e. the impurity is about 2% of the solid content for nanoGEM.SiO<sub>2</sub>.PEG, and less than that for the other variants. These same supernatants (a.k.a. Überstand, Nullprobe) were sterilized and distributed to partners as control for tox assays.

To determine the *ROS activity* (reactive oxygen species) of the SiO<sub>2</sub> nanomaterials, measurements were done by electron paramagnetic resonance (EPR) spectroscopy using two different methods. The SiO<sub>2</sub> nanoGEM materials and likewise the particle-free supernatants show little to no (surface) reactivity. Moderate hydroxyl radical formation potential was observed for all materials tested, including the particle-free supernatants. The observed radical formation is hence not or not only a nano-specific effect related to the particles, but could be related to dissolved impurities.

**Table 1** Overview of the ROS activity for the SiO<sub>2</sub> material analysis expressed as arbitrary units (AU), n = 3

ID	(surface)reactivity (CPH)			OH· (DMPO)		
	yes/no	Mean value ± σ in AU	x-fold increase compared to dH <sub>2</sub> O	yes/no	Mean value ± σ in AU	x-fold increase compared to dH <sub>2</sub> O
SiO <sub>2</sub> PEG 500*	no	8769 ± 1685	1	yes	12820 ± 1796	<b>11</b>
SiO <sub>2</sub> PEG 500 supernatant	yes	113650 ± 12029	<b>3.4</b>	yes	12212 ± 416	<b>13</b>
SiO <sub>2</sub> naked*	yes	46356 ± 1342	<b>4</b>	yes	13140 ± 694	<b>11</b>
SiO <sub>2</sub> naked supernatant	no	19904 ± 3716	0.88	yes	6119 ± 609	<b>6.3</b>
SiO <sub>2</sub> amino	no	8856 ± 298	0.57	yes	17099 ± 1737	<b>21</b>
SiO <sub>2</sub> amino supernatant <sup>1</sup>	no	3360 ± 577	1,1	yes	11443 ± 405	<b>5,2</b>
SiO <sub>2</sub> phosphate	yes	105106 ± 17250	<b>2.2</b>	yes	18817 ± 117	<b>19</b>
SiO <sub>2</sub> phosphate supernatant <sup>1</sup>	no	3937 ± 521	1,2	yes	10949 ± 320	<b>5,0</b>

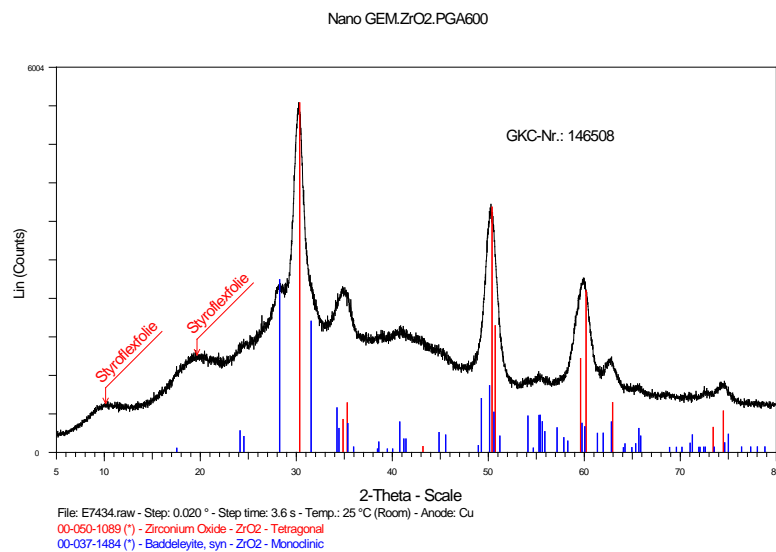
\* n = 6 due to follow-up measurements; <sup>1</sup> supernatant / particle-free suspension medium was not measured.

### 3. Surface functionalized nano-ZrO<sub>2</sub> suspensions from ItN

ItN was responsible for the production of modified crystalline nano-zirconia samples with varying surface modifiers. The for crystallization purposes hydrothermally treated base material (uncoated nano-zirconia) was either semi-technically produced (20kg batches) or was produced in smaller 500g/1000g autoclavation vessels with subsequent surface modification.

The surface of average ca. 10nm large zirconia (mixed crystal phase monoclinic-tetragonal; particles being 3-18nm) was either modified with a caustic polyacrylate (Acrylate), an acidic polyoxocarbonic acid (TODA), with an amino silane (APTS) or with a polyethylen glycol (PEG).

The following picture shows the pure crystal structure which remains unchanged in the course of the surface modification.



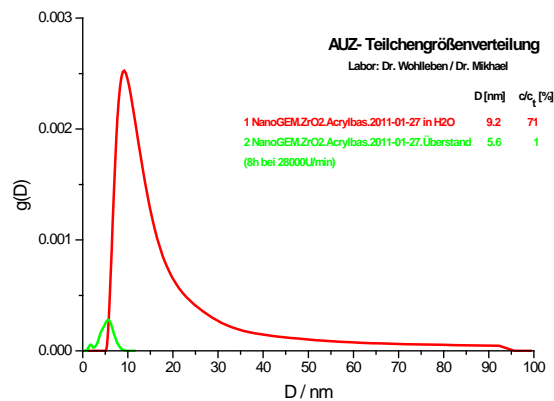
In the earlier Nano-Care project, the polyacrylate and polyoxocarbonic acid (TODS) coated samples were partly introduced as they are already available on a larger scale. They were also provided this time for the project partners due to their availability and were partly characterized. APTS and PEG were completely new though as surface modifying agents and were in the focus of this current deliverable. They are discussed here in more detail than the acrylate or acid modified material.

After preparation and characterization, sterilization of 10% wt% suspensions was done at University of Munster (WWU) before the samples were provided for AP3 partner for toxicological study purposes.

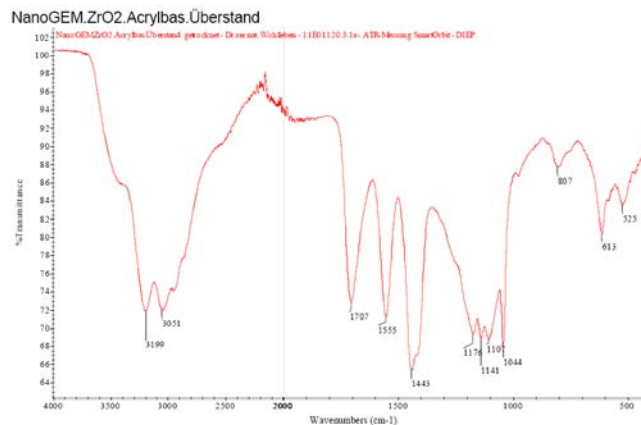
Water based supernatants after ultracentrifugation and pure modifier solutions were also sent to AP3 partners after sterilization.

### Acrylate modified nano-zirconia

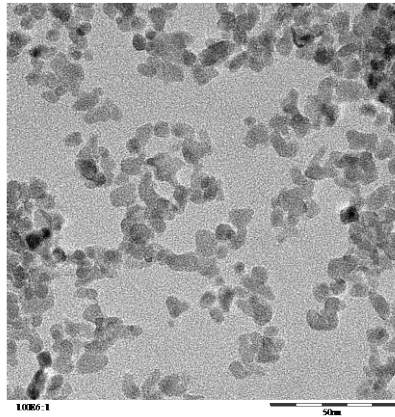
The 10wt% suspension was prepared in water, with the supernatant containing 5nm particles with one percent of the original concentration. The primary crystalline size could be determined as having 9nm for 71% of the particles with agglomerates reaching in the 30-40nm region..



Infrared exhibited traces of acrylic acid and a salt of an acrylic acid. Zetapotential was negative. An IEP could not be measured with the zeta sizer instrument.

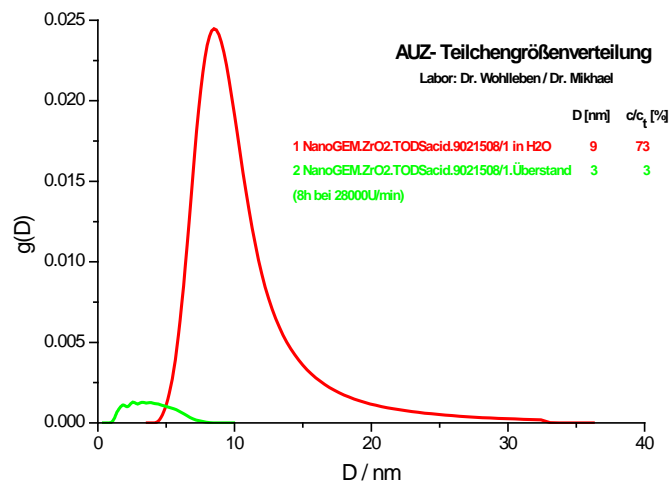


H-TEM showed very well crystallized deagglomerated particles.

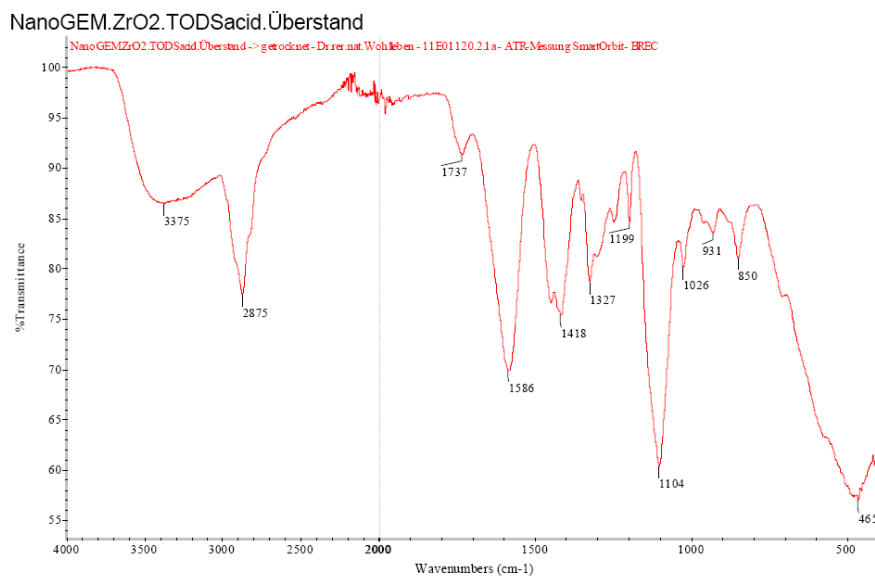
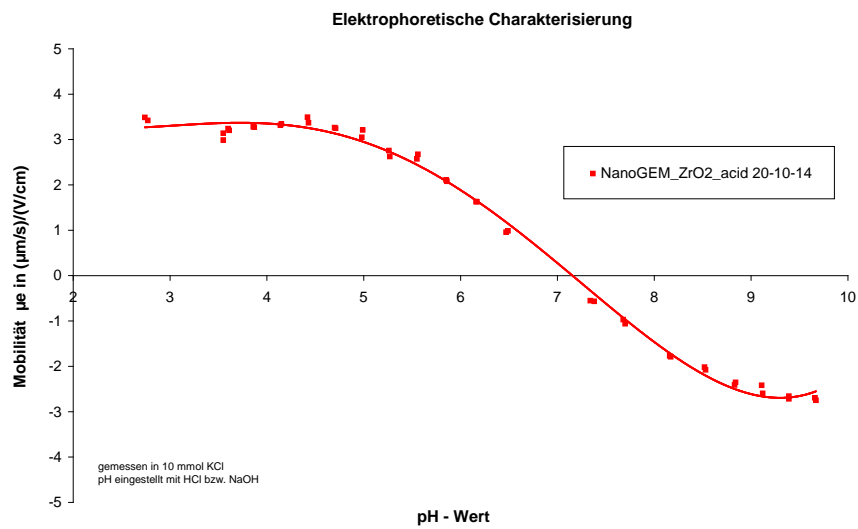


### Acid (TODS- Polyoxocarbonic acid)

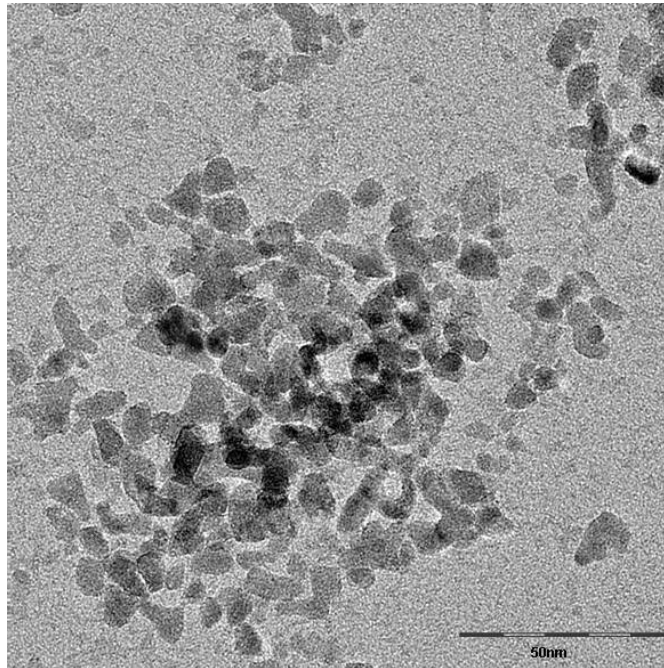
Tri-Oxa-decanoic acid (TODS), a polyoxocarbonic acid was used as an effective surface modifying agent. DLS showed that ca. 73% of particles were ca. 9nm in radius but small agglomerates were identified at ca. 70nm. The supernatant showed 3nm particles with a concentration of ca 3% of the original. That means that 97% of the original particles can be removed by ultracentrifugation.



IEP was found at ca. 7 with IR showing proof of an inorganic oxide and carbonic acid salts with a strongly pH depending curve of the charges.

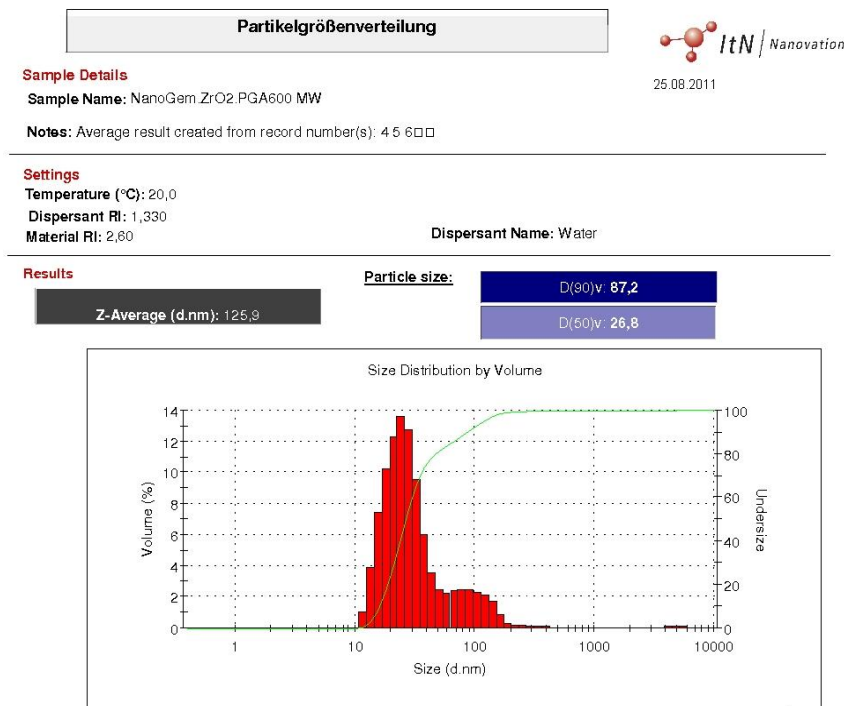


TEM exhibited rather irregularly shaped particles which appear more aggregated than the comparative samples for the acrylate, the APTS and PEG.



### PEG modified nano zirconia

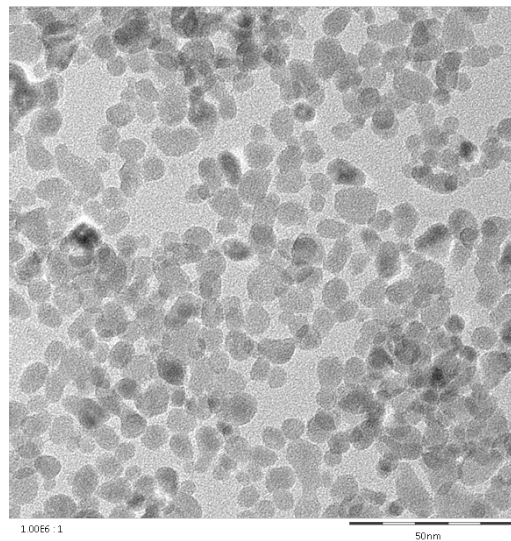
10wt % water based suspensions were prepared using polyglycolic di-acid with a medium chain length of 600g/mol. In suspension this solution showed a bimodal hydrodynamic,



particle size distribution between 10 and 200nm with a  $D_{90}$  of 87nm and a  $D_{50}$  of 27nm. The zeta potential at 20°C is in the range of 36mV with an IEP between 6 and 7.

The following H-TEM picture confirms the primary particle size below 10 and shows well crystallized nearly monodisperse zirconia nano particles. They have a nearly spheroidal shape.

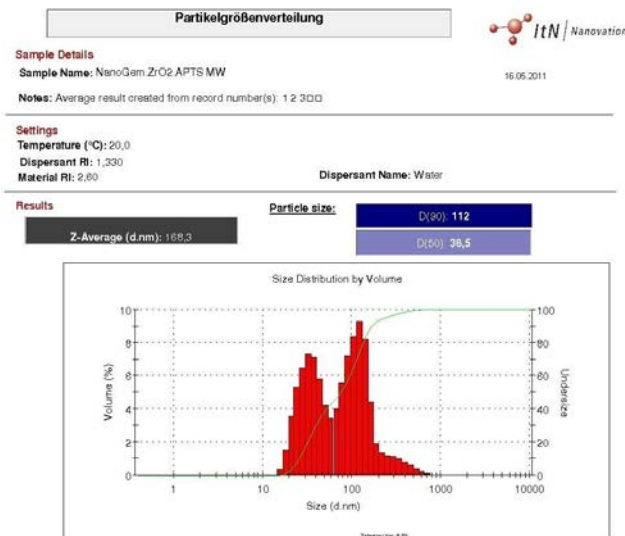
The supernatant shows ca 1.2% of particles left with a mean diameter of ca. 5nm. Pure PEG can also be found and an unidentifiable carbonic acid salt as impurities.



### **APTS modified nano zirconia.**

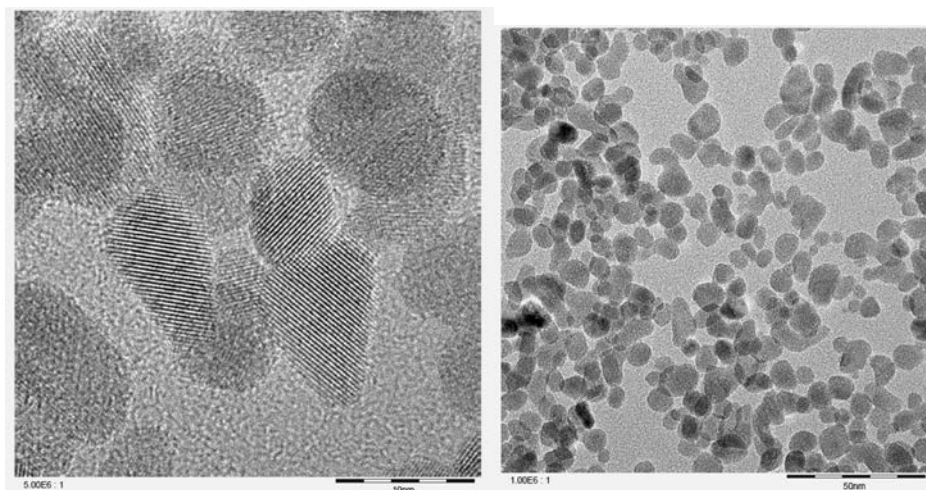
10 wt% water based suspensions were prepared using Aminopropyltrimethoxysilane (APTS) as a caustic modifying agent that couples to the OH groups of the hydrophilic zirconia.

The particle size distribution in water also shows a bimodal distribution with particles having radii between 315 and more than 500nm (probably agglomerates).



Zetapotential being in the range of ca. 30mV at pH = 10. No IEP could be found. The supernatant showed traces of polydimethylsiloxane and a carbonic acid salt, both being probably impurities from the reagents and the actual synthesis.

The following H-TEM pictures of single crystalline particles show a mean primary particle size between 3 and 20, with average in the range of 10nm. Agglomerates are widely absent from the sample.



#### 4. Luminescent nanomaterials: nano-TiO<sub>2</sub>, nano-SiO<sub>2</sub> powders from IUTA

IUTA has synthesized two different luminescent materials. First Europium doped TiO<sub>2</sub> nanoparticles and second Silicon nano particles in a SiO<sub>2</sub> matrix.

##### **Eu doped TiO<sub>2</sub>**

The synthesis of the doped TiO<sub>2</sub> was performed in a flame reactor using the precursor materials Titanetraaisopropoxid (TTIP) and Europiumnitrate as dopant. The material was synthesized with a doping concentration of 5 % Eu under atmospheric conditions.

##### Dynamic light scattering (DLS)

For the DLS analysis the doped TiO<sub>2</sub> particles must be transferred into a stable dispersion. A 0.1 mass-% dispersion of Eu-doped TiO<sub>2</sub> nanoparticles was prepared in water at pH = 2 (HCl) and treated with an ultrasonic probe with a power of 200 watts. Experiments at higher pH values did not provide satisfactory results with respect to the stability of the dispersions.

By this treatment, a reduction of the agglomerate size and the homogenization of the dispersion is achieved. The size of the agglomerates usually depends on the time of treatment, subsequently the irradiation time has been varied (60, 90 min and 120 min). The results of the DLS (Figure 4.1 a-c) measurements (each sample was measured 5 times) on the created dispersions is shown below.



**Nanoparticulate Europium-doped TiO<sub>2</sub> powder**

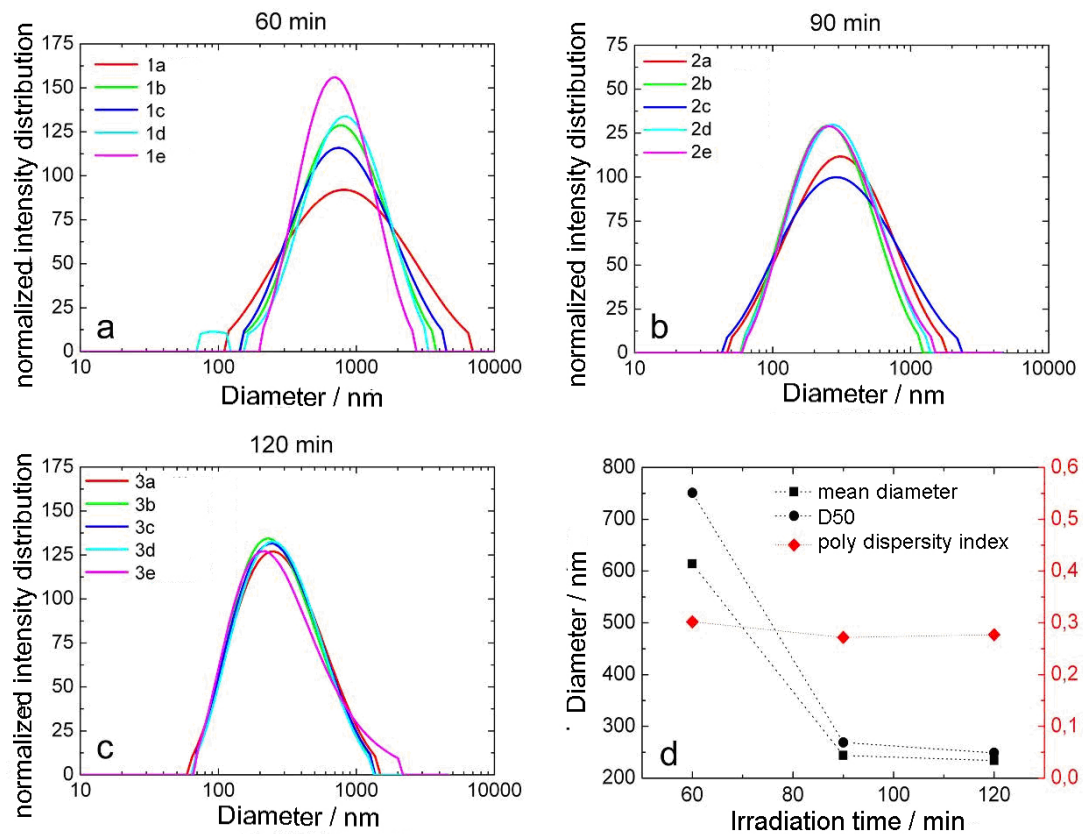


Figure 4.1: The results reveal that the mean diameter does not change significantly after 90 minutes of US treatment and that the polydispersity index is not significantly influenced by the treatment.

BET analysis (gas adsorption on surface) reveals a specific surface area of 208 m<sup>2</sup>/g corresponding to a particle diameter of 6.8 nm (calculation of particle size under the assumption spherical particles).

### Luminescence

The investigations by fluorescence spectrometry showed that the europium can be directly excited at a wavelength of 464 nm and can also be stimulated with energies above the band gap of TiO<sub>2</sub>. The typical emission spectrum is shown below. The spectral position of the inter-atomic transitions of europium is allocated by marking the corresponding wavelengths (in nm). The results indicate that the optically active incorporation of europium was successfully performed.

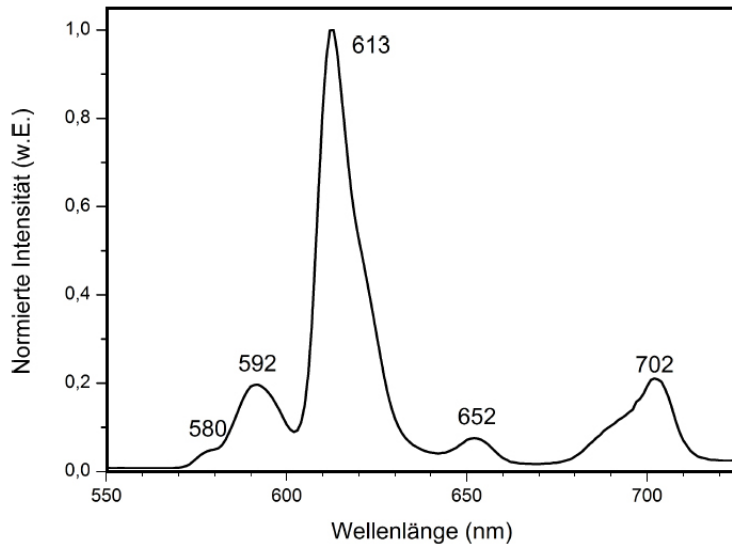


Figure 4.2: Photoluminescence signal of Europium-doped TiO<sub>2</sub> at a excitation wavelength of 464 nm

### Electron microscopy

SEM investigation on nanoparticulate layers created by dispensing of the dispersions described earlier on silicon substrates reveal a continuous layer of particles containing single particles in the size regime of 100 nm (Figure 4.3a). EDX analysis of these layers reveal the incorporation of Eu into the particles. This fact was especially proved for bigger particles, due to the resolution of the EDX-detector. Presumably, the Eu signal was too poor to receive information from layer - areas consisting of small particles (Figure 4.3b).

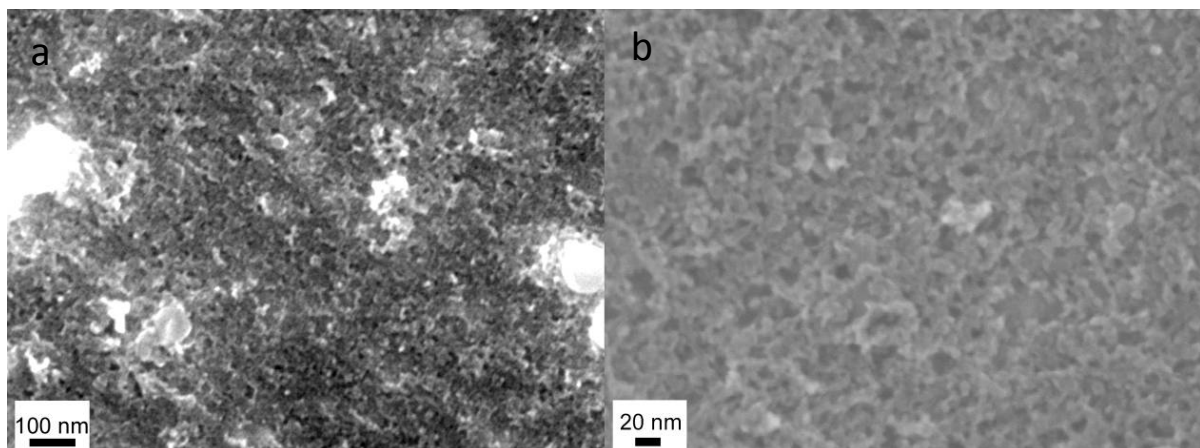


Figure 4.3 SEM images of a layer of doped TiO<sub>2</sub> particles, right: magnification

### Production of Silicon Quantum Dots

The preparation of Si crystallites in a SiO<sub>2</sub> matrix has been performed by the use of silane and oxygen in a microwave plasma reactor. For the successful production of SiO<sub>2</sub>-containing Si, the ratio of oxygen and silane was varied. Table 4.1 shows the flow rates and the ratio of the injected gases.

Standard-Liter per Minute	Sample 1	Sample 2	Sample 3	Sample 4	Sample 5
O <sub>2</sub>	0.2	0.35	0.5	0.7	1
SiH <sub>4</sub>	0.25	0.25	0.25	0.25	0.25
O <sub>2</sub> /SiH <sub>4</sub>	0.8	1.4	2	2.8	4

Table 4.1: Overview on the process conditions within the plasma reactor.

The silane is decomposed within the plasma and reacts under the influence of oxygen.



The generated materials were thermally annealed under nitrogen and synthetic air atmospheres. While the temperature was set between 600°C and 800°C, the annealing was varied between 3 h and 6 h.

### Charakterisierung der Materialien

The synthesized materials were characterized using the BET method, DLS and PL spectroscopy.

#### BET

BET investigation on the as-prepared materials show an increasing specific surface area with increasing oxygen content during synthesis. Measurements on annealed materials reveal smaller specific surface areas compared to the starting materials. Furthermore, the annealing time and the applied temperature also influence the specific surface area. It can be stated that with increasing sintering time the specific surface area slightly decreases and with increasing temperature the specific surface area strongly decreases, too.

## DLS

To analyze the agglomerate of the as-prepared and annealed samples dispersions of 0.1-mass % in Isopropanol were sonicated for up to 120 minutes. Subsequently the materials were analyzed via DLS. Figure 4.4 shows the Data for the as prepared material compared to material, which was annealed at 800 C for 6 hours. The data reveal a small impact of the sonication time on the agglomerate size. However, the analysis of measurements shows an increase of agglomerate size due to the thermal treatment.

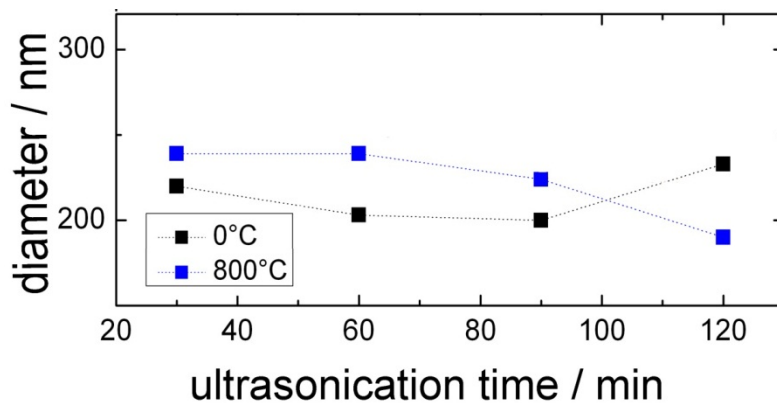


Fig 4.4: Agglomerate size of as-prepared and annealed Si/SiO<sub>2</sub> for different ultrasonication times

### Photoluminescence

PL measurements on the as-prepared material (Sample 1 -5) show that the increase of the oxygen content during the synthesis leads to a shift of the emission maximum of the photoluminescence to smaller wavelengths. Since the emitted light was still above the visible light spectrum for all samples a thermal post treatment was applied under N<sub>2</sub> and synthetic air atmosphere. While the treatment under N<sub>2</sub> atmosphere does not influence the wavelengths of the emitted light significantly, the thermal treatment under synthetic air leads to a shift of the maximum of the PL signal to smaller wavelengths. This shift is associated with a decrease of the Si crystallites size, due to the conversion of Si into SiO<sub>2</sub>.

Therefore, detailed investigation was performed on sample 5 after thermal treatment at different temperatures in synthetic air. Additionally the duration of treatment was varied. Here, the starting material in a total of 9 different process conditions were aftertreated. The temperature was adjusted to 600 ° C, 700 ° C or 800 ° C, and in all cases processed with different times (4 h, 5 h and 6 h). The thus prepared samples were characterized by photoluminescence studies (PL).

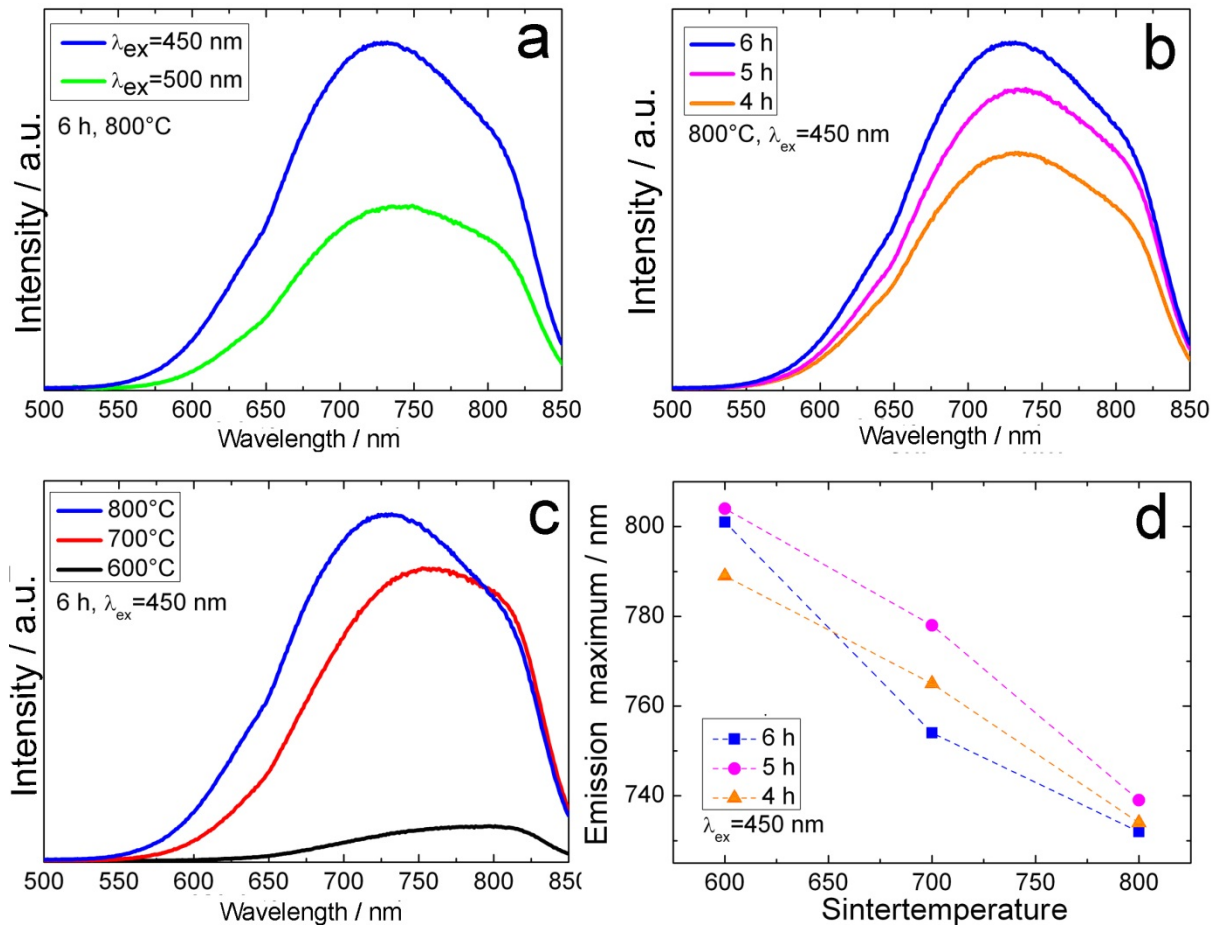


Figure 4.5a-d: PL studies of thermally post-treated SiO<sub>2</sub>@Si: (a) Comparison of the PL intensity at excitation wavelength of  $\lambda = 450$  nm and  $\lambda = 500$  nm, (b): Effect of sintering time on the PL signal, (c) Influence of the sintering temperature on the PL signal, (d): wavelengths of maximum PL intensity as a function of the sintering temperature for different process times

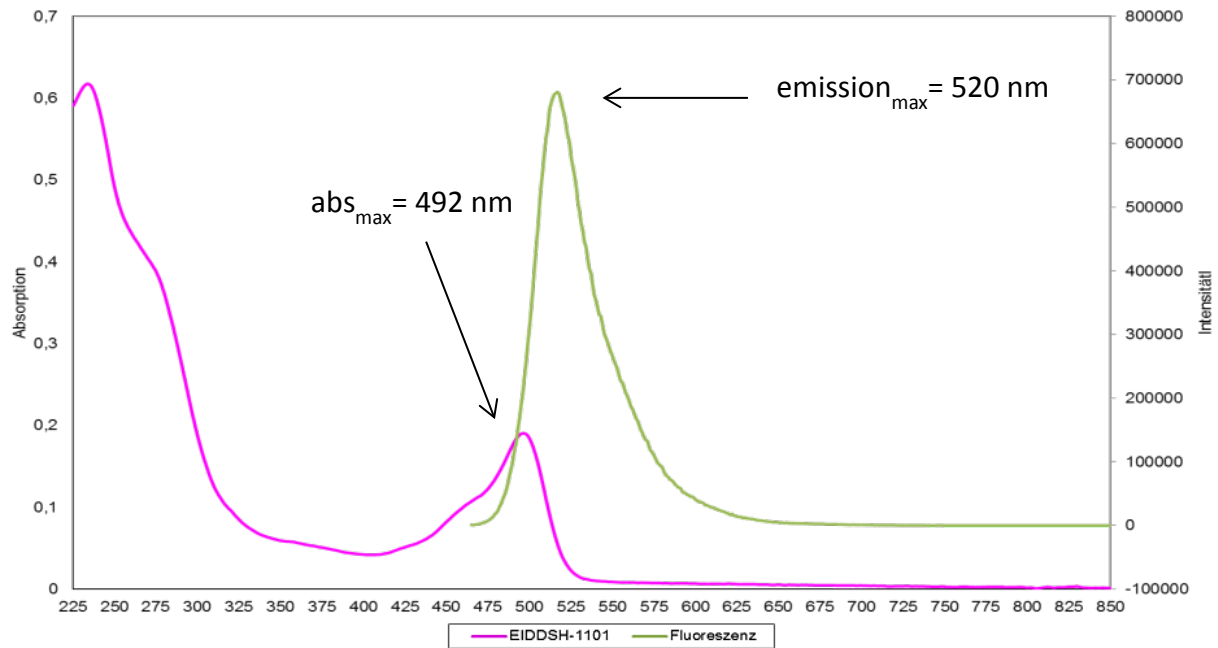
For the first measurements excitation wavelengths of 450 nm and 500 nm are set at sample 5 (post-treated at 800 ° C, 6h). Figure 4.5a shows the PL signal at different wavelengths. Due to the expected increase in signal intensity at a wavelength of  $\lambda = 450$  nm, the following studies were carried out at this wavelength.

Figure 4.5b shows the influence of the sintering time on the PL signal. The measurements show that the sintering time slightly shifts the position of the maximum. Figure 4.5c displays the influence of the position of the maximum on sintering temperature, the measurements show a shift of the maximum to smaller wavelengths and ,thus, in the direction of the visible light spectrum. Figure 4.5d shows the wavelength of maximum PL intensity as a function of the sintering temperature for different process times. The largest displacement effect could be

achieved by a thermal treatment at 800 °C and for 6 h processing time. Accordingly, the post-treatment under the influence of oxygen at higher temperatures leads to an increased conversion of Si to SiO<sub>2</sub> and to an associated reduction in the Si crystallite size within the sample.



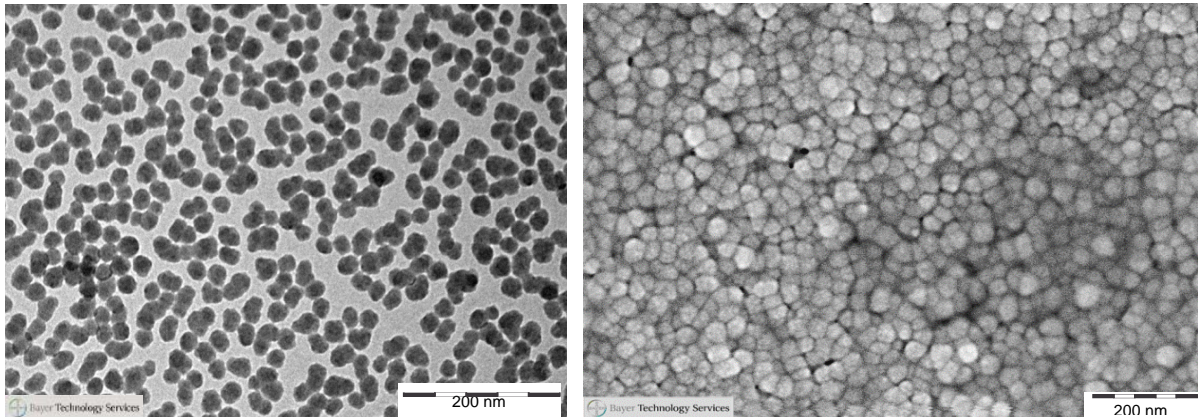
The fluorescence properties of the core/shell NPs were assessed with spectrofluorometry. The absorption and emission spectra indicated the NPs fluorescence even after coating with non-fluorescent shell.



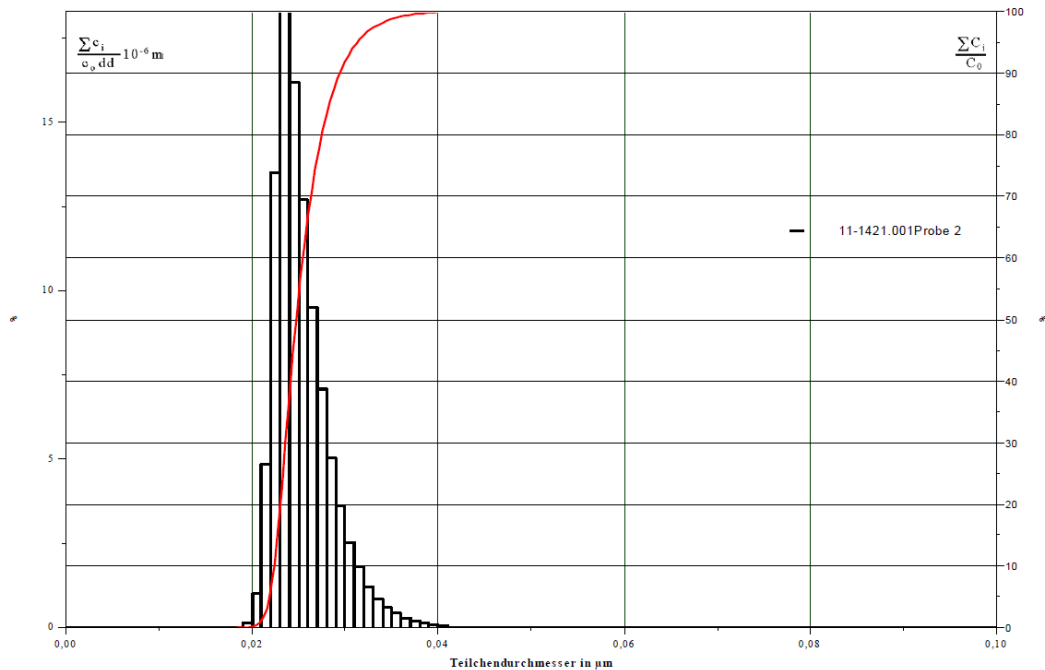
The results of the NPs characterization are summarized below:

Name	SiO <sub>2</sub> _FITC
Shape	Spherical
Concentration	13.8 % (wt/wt)
Specific surface area	1.78*10 <sup>2</sup> m <sup>2</sup> /g
pH	8.7
Size/size distribution & aggregation/agglomeration state	DLS: 32.5 nm +/-2.6*; PDI= 0.065 TEM: d <sub>50</sub> = 25 nm, d <sub>90</sub> = 28 nm AC: d <sub>50</sub> = 25 nm, d <sub>90</sub> = 29 nm
Crystal structure	amorphous
Surface chemistry	XPS: Atom % O 63.3, Si 29.1, C 7.7 SIMS: Si <sub>x</sub> O <sub>y</sub> , Ca, K
Surface charge	- 38.83 mV +/- 1.99; IEP: 3.5

SEM and TEM images showed a spherical shape and monodispersity of the NPs after the shell synthesis:



The monodispersity was additionally proven with AUC:



SIMS spectra analysis indicated that the fluorescent FITC-APTES complex was incorporated within the NPs. There were no characteristic picks of FITC observed on the NPs surface. The spectra showed only a presence only of FITC fragments. This can be caused by the NPs ‘explosion’ after their exposure to the light beam.

## 6. Methods for characterization

### **Dynamic Light Scattering/Zeta Potential**

The particles hydrodynamic size/size distribution and zeta potential were measured by a Zetasizer 3000 HSA and a Zetasizer Nano ZS, Malvern Instruments. The NPs size was assessed by dynamic light scattering (DLS) technique using a He-Ne laser (633 nm) as the light source. The stock suspension was diluted with deionized water to result in a count rate of 100-500 kcps. Particle sizing measurements were performed in 10 mm polystyrene cuvettes at 25°C. The results were given as Z-average values of number, volume and intensity size distribution. The zeta potential was determined by Laser Doppler Electrophoresis (LDE) using a quartz capillary electrophoresis cell. Nanoparticles were dispersed in deionized water with a concentration of 10 mg/ml and incubated for 30 min in an ultrasonic water bath at room temperature.

All of the measurements were triplicated for a single batch of NPs and the results were the average of the three measurements.

### **Analytical Ultracentrifugation**

The turbidity-AUC machine was used for the IUTA and BTS data sheets. For the BASF and ItN data sheets, an interference-AUC machine was used. Both rely on the identical principle of 'detection during fraction'.(Planken and Colfen 2010; Wohlleben 2012)

turbidity-AUC: The particle size distribution was additionally determined by a Beckman Ultracentrifuge type XL70, equipped with an optical device. As the light source a diode laser (695 nm) with an optical fiber was used. A photodiode detector was connected to an analog digital converter. For the analysis, a 3-mm Beckman quartz cell was used with a gap having a width of about 0,3 mm for the passage of the light. The samples were diluted to obtained concentrations ranging from 0,5-0,05 %. Depending on the particles size, the samples were centrifuged for 10-120 min at speed of 4000 to 50000 U/min.

interference-AUC uses Beckman Ultracentrifuge type XLI with integrated interference optics. The actual particle concentration is read directly from the optical fringe shift without necessity of Mie conversion or other correction. The size distribution is evaluated by the freeware program Sedfit, with fitting model ls g(s\*).(Schaefer et al. 2012; Wohlleben 2012)

### **Transmission Electron Microscopy**

The primary NPs size and shape were assessed using a Phillips CM20 transmission electron microscopy (TEM) working at 200 keV. For TEM analysis, stock nanoparticle suspensions were diluted in deionized water to the final concentration of 0,1 mg/ml. Three  $\mu\text{l}$  were pipetted onto holey carbon grids (S162, Plano GmbH) and subsequently left to evaporate. A series of images were selected to estimate particle size/size distribution using the analySiS pro software.

The crystal structure and crystalline appearance was visualized using TEM-imaging on a Jeol JEM-3010 TEM operating at 300 keV. In this case, a carbon coated 300 mesh TEM grid was dipped into a dispersion with a concentration of 0,1 mg/ml in isopropanol.

### **Scanning Electron Microscopy**

The primary NPs size and shape were additionally assessed using a FEI Sirion 100 T scanning electron microscopy (SEM) working at 10 keV. For SEM analysis, 20  $\mu\text{l}$  stock suspensions were dried directly on the carbon adhesive pad of a SEM sample holder.

### **X-ray Photoelectron Spectroscopy**

The chemical and elemental composition of NPs were examined with a PHI VersaProbe 5000 scanning X-ray photoelectron spectroscopy (XPS), using a monochromated Al  $K\alpha$  X-ray beam scanned over  $600\mu\text{m} \times 400\mu\text{m}$  area (200 $\mu\text{m}$  diameter / 50W X-ray beam) or  $1400\mu\text{m} \times 100\mu\text{m}$  (100 $\mu\text{m}$  diameter / 100W X-ray beam ) at a fixed take-off angle  $45^\circ$ . For XPS analysis, the stock suspensions were dried on an indium or silicon surface. Spectra evaluation was performed using MultiPack-Version 9.2. software.

Impurities and surface modification were also determined by a PHI XPS 5500 system equipped with 300 W monochromatic Al  $K\alpha$  radiation. The pass energy for surveys was 117 eV (measurement time of 45 min) and for detailed spectra 23.5 eV (measurement time of 6 min). In this case, spectra evaluation was performed by CasaXPS 2.3.15, based on the PHI standard-sensitivity factors, with Shirley background subtraction and peak shape fits as sum of 90 % Gaussian and 10 % Lorentzian. Information depth was limited to the surface 10 nm of the material. Two measurements per sample were performed, each integrating over 0.5  $\text{mm}^2$ . The results in % are derived from relative concentration of elements and their chemical bonds from line shape analyses.

### **Time-of-Flight Secondary Ion Mass Spectrometry**

The surface chemistry measurements were performed using a time-of-flight secondary ion mass spectrometer IV (ToF-SIMS, Iontof GmbH, Germany). The primary ion species used as 10 keV Ga<sup>+</sup>, scanning an area of typically 150 x 150 μm<sup>2</sup>. Static TOF-SIMS spectra were additionally recorded using a ToF-SIMS V spectrometer. In this case, a pulsed mass-filtered primary ion beam of 25 keV singly charged bismuth (Bi<sup>+</sup>) was used. This primary ion beam, resulting in a spot size of typically 5 μm on the sample surface, was raster scanned over an area of 250x250 μm<sup>2</sup> to record spectra of positive and negative secondary ions. The rastered area integrates over more than 10<sup>6</sup> particles. The primary ion dose density was always kept well below 10-12 ions/cm<sup>2</sup>. To prevent charging of the sample surface, a low-electron energy flood gun was used. The sample particle sediments were prepared for SIMS analysis by their placing on clean silicon wafers.

### **X-ray Diffraction**

Crystallite size and crystalline phase were evaluated by X-ray reflexion diffractometer (XRD) PANalytical EMPYREAN PIXcel with 3D Counter operating at a voltage of 40 kV and a current of 40 mA with Cu K $\alpha$  and K $\beta$  radiation. For XRD analysis, the stock suspensions were dried on a silicon surface. Alternatively, for SiO<sub>2</sub> and ZrO<sub>2</sub>, crystallinity was also determined by a D8 Advance (Fa. Bruker/AXS) as function of the diffraction angle ( $2^\circ < 2\theta < 150^\circ$ ). Quantitative phase analysis was performed using Rietveld refinement.

### **BET-Specific surface area**

Specific surface area was determined using BET method<sup>3</sup>, from nitrogen adsorption /desorption isotherms, recorded at 77 K on Gemini 2360 (Micromeritics S/N 3014). The measuring range was 0,1-1000 m<sup>2</sup>/g. The stock solution was previously freeze dried to obtain 0,5 g of the examined sample.

### **Nanoparticles concentration**

NPs concentration was additionally analyzed with Halogen Moisture Analyzer (Mettler Toledo, HR73). 1 g of the stock solution was placed onto an analyzer plate and left for the solvent evaporation to give the wt/wt % value.

---

<sup>3</sup> Brunauer S, Emmett PH, Teller E: Adsorption of gases in multimolecular layers. *J. Am. Chem. Soc.* 1938, 60: 309-319.

### **ROS (reactive oxygen species) activity – text for materials & methods in publications**

ROS activity (reactive oxygen species) measurements were done by electron paramagnetic resonance (EPR) spectroscopy using two different methods. Employing the method of Pappageorgiou et al (2007), that uses CPH (1-hydroxy-3-carboxy-pyrrolidine) as spin probe possible (surface)reactivity was investigated. Additionally, employing the method of Shi et al (2003) the potential hydroxyl radical (OH·) formation in the presence of hydrogen peroxide (H<sub>2</sub>O<sub>2</sub>) and the spin trap 5,5-dimethyl-1-pyrroline-N-oxide (DMPO) was determined.

The assessment of the potential ROS activity is done by taking the response of deionized water (dH<sub>2</sub>O) as reference signal and assuming a 30% uncertainty of the measurement methodology. Since this uncertainty varies from one material to another, based on experience, a 1.3-fold increase in the signal intensity compared with the signal of dH<sub>2</sub>O is considered as a significant ROS activity in this study. This assessment factor serves as a guideline and not specifically as absolute assessment criteria.

Prior investigations within this project showed no significant differences in the ROS activity of selected materials after different dispersion methods, e.g. vortexing for 1 min, or stirring for 1 h, respectively 24 h. Consequently, 1 minute vortexing was used as dispersion procedure prior their EPR analysis measurements. Some more information on the differences between the DMPO and CPH probe are given in the German version of this deliverable.

## 7. References

Borm PJA; Kelly F; Künzli N; Schins RPF & Donaldson K (2007): Oxidant generation by particulate matter: from biologically effective dose to a promising new metric. *Occupational and Environmental Medicine*, 64:73-74.

Donaldson K; Stone V; Borm PJ; Jimenez LA; Gilmour PS; Schins RPF; Knaapen AM; Rahman I; Faux SP; Brown DM & MacNee W (2003): Oxidative stress and calcium signalling in the adverse effects of environmental particles (PM10). *Free Radical Biology and Medicine*, 34(11):1369-1382.

ECHA. Guidance on information requirements and chemical safety assessment: Appendix R7-1 Recommendations for nanomaterials applicable to Chapter R7a - Endpoint specific guidance - ECHA-12-G-03-EN . 30-4-2012.

Ref Type: Online Source

Nel A; Xia T; Madler L & Li N (2006): Toxic potential of materials at the nanolevel. *Science*, 311:622-627.

OECD (2009) Guidance Manual for the Testing of Manufactured Nanomaterials: OECD Sponsorship Program.

Papageorgiou, I; Brown, C; Schins, R; Singh, S; Newson, R; Davis, S; Fisher, J; Ingham, E; Case, CP (2007): The effect of nano- and micron-sized particles of cobalt chromium alloy on human fibroblasts in vitro. *Biomaterials* 19: 2946-2958.

Planken KL, Colfen H (2010) Analytical ultracentrifugation of colloids. *Nanoscale* 2:1849-1869.

Schaefer J, Schulze C, Marxer EEJ, Schaefer UF, Wohlleben W, Bakowsky U, Lehr CM (2012) Atomic Force Microscopy and Analytical Ultracentrifugation for Probing Nanomaterial Protein Interactions. *ACS Nano* 6:4603-4614.

Schaumann F; Borm PJA; Herbrich A; Knoch J; Pitz M; Schins RPF; Luettich B; Hohlfeld JM; Heinrich J & Krug N (2004): Metal rich ambient particles (PM2.5) cause airway inflammation in healthy volunteers after segmental instillation. *American Journal of Respiratory and Critical Care Medicine*, 170:898-903.

Shi T; Duffin R; Borm PJA; Li H; Weishaupt C & Schins RPF (2006): Involvement of hydroxyl radical generation in particulate matter induced DNA damage. *Environmental Research*, 101:18-24.

Shi, T; Schins, RPF; Knaapen, AM; Kuhlbusch, T; Pitz, M; Heinrich, J & Borm PJA (2003): Hydroxyl radical generation by electron paramagnetic resonance as a new method to monitor ambient particulate matter composition. *Journal of Environmental Monitoring*, 5, 1-8.

Wohlleben W (2012) Validity range of centrifuges for the regulation of nanomaterials: from classification to as-tested coronas. *J Nanopart Res* 14:1300.

Wohlleben W, Ma-Hock L, Boyko V, Cox G, Egenolf H, Freiberger H, Hinrichsen B, Hirth S, Landsiedel R (2013) Nanospecific guidance in REACH: A comparative physicalchemical characterization of 15 materials with methodical correlations. *J Ceramic Sci Technol* , in print..